# Zero- to ultralow-field NMR spectroscopy of small biomolecules

Piotr Put,[†] Szymon Pustelny,[†] Dmitry Budker,[‡,¶] Emmanuel Druga,[§] Tobias Sjolander,[§] Alexander Pines,[§] and Danila Barskiy[*,‡,§]

†*Smoluchowski Institute of Physics, Jagiellonian University in Kraków, Kraków, Poland*
‡*Helmholtz-Institut Mainz, Johannes Gutenberg-Universität, 55099, Mainz, Germany*
¶*Department of Physics, University of California, Berkeley, CA 94720, USA*
§*Department of Chemistry, University of California Berkeley, Berkeley, CA, 94720, USA*

E-mail: dbarskiy@uni-mainz.de

## Abstract

Nuclear magnetic resonance (NMR) spectroscopy is a well-established analytical technique used to study chemicals and their transformations. However, high-field NMR spectroscopy necessitates advanced infrastructure and even cryogen-free benchtop NMR spectrometers cannot be readily assembled from commercially available components. We demonstrate construction of a portable zero-field NMR spectrometer employing a commercially available magnetometer and investigate its applications in analytical chemistry. In particular, $J$-spectra of small representative biomolecules [$^{13}$C]-formic acid, [1-$^{13}$C]-glycine, [2,3-$^{13}$C]-fumarate, and [1-$^{13}$C]-D-glucose were acquired and an approach relying on the presence of a transverse magnetic field during the detection was investigated for relaxometry purposes. We found that water relaxation time strongly depends on the concentration of dissolved D-glucose in the range of 1-10 mM suggesting opportunities for indirect assessment of glucose concentration in aqueous solutions. Extending analytical capabilities of zero-field NMR to aqueous solutions of simple biomolecules (aminoacids, sugars and metabolites) and relaxation studies of aqueous solutions of glucose highlight the analytical potential of non-invasive and portable ZULF NMR sensors for applications outside of research laboratories.

## Introduction

In recent years, zero- to ultralow-field (ZULF) nuclear magnetic resonance (NMR) emerged as a complementary approach to traditional, high-field NMR techniques.[1–6] In contrast to conventional high-field NMR, in ZULF NMR experiments nuclear spin evolution occurs under dominant intermolecular interactions such as $J$ couplings while the Zeeman interaction acts only as a small perturbation to the system. Under such conditions, nuclear magnetization evolves at low frequencies (1-500 Hz), thus, magnetometric techniques alternative to conventional inductive pickup coils are required to detect NMR signals.[7]

A specific example of devices capable of detecting low-frequency oscillating magnetic signals are optically-pumped magnetometers (OPMs). OPMs detect magnetic fields via monitoring properties of light propagating through a magnetically active medium, e.g., alkali-metal vapor enclosed in a glass cell. For ZULF NMR purposes, an OPM comprising a vapor cell is brought to proximity with a sample under study, and the evolution of nuclear spins from the sample is probed by the OPM via detection

of the magnetic field produced by the nuclear spins. OPMs are capable of detecting magnetic fields with femtotesla sensitivity (1-10 fT/$\sqrt{\text{Hz}}$) without use of cryogenics and nearly no maintenance. Moreover, OPM devices are currently available commercially.[8]

ZULF NMR employing OPMs is used to distinguish chemicals in the liquid state based on their unique nuclear-spin topology and $J$ couplings,[9–11] also allowing characterization of chemically exchanging systems[12] and monitoring chemical reactions.[13] Multidimensional ZULF NMR spectroscopy is also being developed[14] as the methodological portfolio of tools available at zero field continues to grow.

Despite the formidable progress achieved in recent years, many demonstrations of the ZULF NMR spectra were still performed on home-built devices that require relatively sophisticated optical equipment. In this paper, we showcase a portable zero-field NMR spectrometer that employs a commercially available magnetometer QuSpin-QZFM and describe its use for the analysis of small biomolecules [$^{13}$C]-formic acid, [1-$^{13}$C]-glycine, [2,3-$^{13}C_2$]-fumarate and [1-$^{13}$C]-D-glucose in solution. We specify a simple arrangement of the experiment in which both $J$-spectra and nuclear spin relaxation can be employed for the analytical chemistry purposes. Relaxometry of the aqueous solutions of glucose in a physiological concentration range (0-10 mM) is performed highlighting potential of non-invasive and portable ZULF NMR sensors for applications outside of laboratory. Studies are under way towards the detection of biomolecules in vivo and/or in situations where conventional high-field NMR detection is not possible or challenging to carry out.

# Results and discussion

## Magnetization precession at ultralow fields

Operation under ZULF conditions provides complementary information about nuclear spin systems compared to that of high-field NMR. In general, two groups of resonances may be identified in ZULF NMR spectra when the initial magnetization is oriented along the sensitive axis of the magnetometer and a small (10-50 nT) field is applied perpendicular to the sensitive axis (Fig. 1). The first group of resonances, akin to high-field NMR measurements, arises due to the Larmor precession of magnetization caused by the Zeeman interaction with the transverse magnetic field. In ZULF NMR spectra, these resonances are typically observed at frequencies up to several hertz.

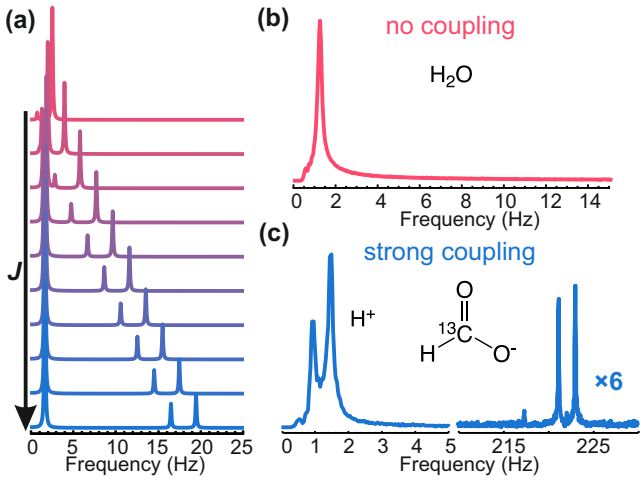


Figure 1: (a) Simulation of ultralow-field spectra of a two-spin system ($^1$H-$^{13}$C) subjected to a weak external magnetic field (50 nT) oriented perpendicular to the sensitive axis of the magnetometer. The spectra are calculated for different values of the $J$-coupling constant (0-18 Hz). (b) Experimentally measured ZULF NMR spectrum of $H_2O$ at a transverse magnetic field of ∼28 nT. (c) Experimentally measured ZULF NMR spectrum of [$^{13}$C]-formic acid at a transverse magnetic field of ∼35 nT. Note the presence of two distinct near-zero-frequency peaks corresponding to the Larmor precession of magnetization in the $^1$H-$^{13}$C system and free acidic hydrogen spins.

The second group of resonances is usually observed at higher frequencies, i.e., at integer or half multiples of the heteronuclear $J$-couplings, depending on the nuclear spin topology of molecules under investigation. The same topology is responsible for the position, number, and strength of the observed peaks unless relaxation or chemical exchange effects cause

the peaks to broaden and/or disappear.

An example of a ZULF NMR spectrum simulated for a simple AX ($^1$H-$^{13}$C) spin system and investigated at nonzero transverse magnetic field (50 nT) with different coupling constants is shown in Fig. 1(a). Without the scalar coupling (top spectrum), only two resonances, arising due to the Larmor precession of $^1$H and $^{13}$C spins, are observed. Nonzero $J$-coupling value modifies the spectra. First, instead of the two Larmor peaks at low frequencies, a single resonance at the mean of the the Larmor frequencies of $^1$H and $^{13}$C is observed. Second, several peaks arise at higher frequencies; when the field is applied perpendicular to the initial magnetization, two peaks are positioned about the $J$-coupling value separated by the sum of the Larmor frequencies of $^1$H and $^{13}$C.

The experimental spectra to demonstrate the two extremes (no coupling vs. strong coupling) are shown for the samples of water and formic acid [Fig. 1(b,c)]. The water spectrum reveals only a single peak at low frequency, $\nu = \gamma_{1H} \cdot (28\ \mathrm{nT}) = 1.2\,\mathrm{Hz}$ [Fig. 1(b)]. This is due to the fact that only $^1$H contribute to the NMR (Zeeman) evolution and no heteronuclear $J$-coupling is present in the system. In the spectrum of neat [$^{13}$C]-formic acid two groups of resonances are observed [Fig. 1(c)]. The low-frequency group consists of one resonance at the mean of the $^1$H and $^{13}$C Larmor frequencies, corresponding to the $^1$H-$^{13}$C backbone of the molecule, and additional resonance at the proton Larmor frequency, corresponding to acidic hydrogens. The high-frequency signals consist of a doublet centered at the $J$-coupling value ($J = 222.2\,\mathrm{Hz}$) and split due to the transverse magnetic field.[15]

Magnetization-precession measurements under ZULF conditions may be useful, as they are straightforward and do not rely on the presence of heteronuclear couplings in molecules. Moreover, a straightforward extension to relaxometry measurements is readily possible[16] (see below). It is also possible to separate overlapping resonances with various multiplicity in $J$-spectra.[3] It is worth noting that measurement under such fields may be challenging for OPMs, since their sensitivity is maximized at zero magnetic field.[17] For example, the QuSpin magnetometer, used in this work, can operate optimally only with the background fields smaller than ∼100 nT, corresponding to proton Larmor precession frequency of roughly 4 Hz. Moreover, OPMs can suffer from worse performance at the low-frequency range caused by technical noise originating from instability of the heater, laser, current sources, etc.[18]

## Zero-field $J$-spectroscopy

Instead of relying on Larmor precession, one can directly detect evolution of nuclear-spin magnetization due to scalar $J$-couplings. In the simple case of two $J$-coupled nuclei, the signal is proportional to the difference between gyromagnetic ratios of these nuclei which means that only heteronuclear coupling can be used for detecting $J$-spectra at zero field. The spectra for a number of different spin topologies were presented and analyzed in a number of papers.[10,19,20]

Figure 2 shows zero-field $J$-spectra of several small biomolecules: (a) amino acid [1-$^{13}$C]-glycine, (b) a metabolite [2,3-$^{13}C_2$]-fumarate, and (c) monosaccharide [1-$^{13}$C]-D-glucose. The $J$-spectra were obtained by sudden transport from high field to zero-field. Before measurements, the residual magnetic fields at the detection region were nullified using a shimming procedure described in Supporting Information (SI). The shuttled samples were contained in evacuated flame-sealed glass tubes.

[1-$^{13}$C]-glycine comprises an effective $A_2X$ spin system and gives a single peak at $(3/2)J$ [Fig. 2(a)]. The $^{14}$N nucleus is effectively decoupled from the rest of the spin system due to its short relaxation time but causes broadening due to scalar relaxation of the second kind.[21]

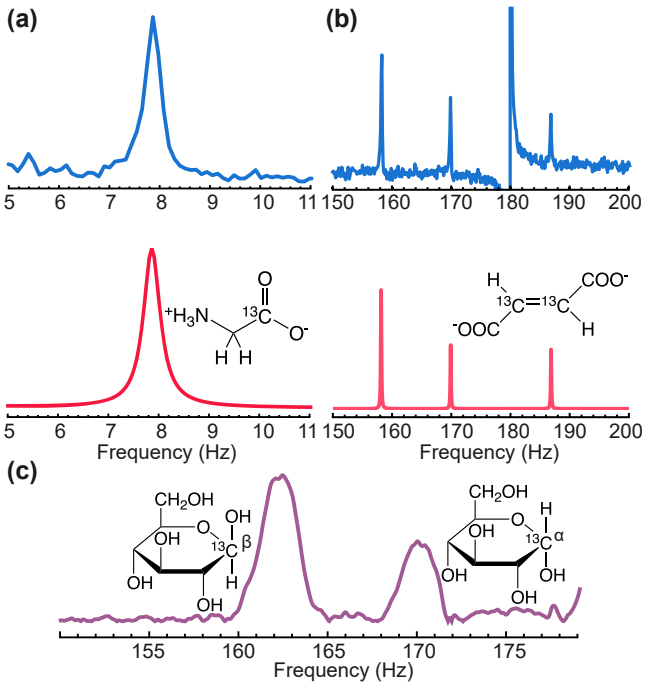


Figure 2: Zero-field $J$-spectra of (a) [1-$^{13}$C]-glycine, (b) [2,3-$^{13}C_2$]-fumarate, and (c) [1-$^{13}$C]-D-glucose. In (a) and (b), top pictures show experimental spectra after averaging (1024 scans) and the bottom spectra are simulations obtained in Mathematica using the SpinDynamica package.[22] In (c), the spectrum is a result of 2000 averages. The peak at 180 Hz comes from residual magnetic field at the power-line harmonic leaking into the magnetic shielding.

The spectrum of [2,3-$^{13}C_2$]-fumarate is more complicated and consists of three main lines around $^{13}$C-$^{13}$H as expected from a numerical simulation [Fig. 2(b)]. [2,3-$^{13}C_2$]-fumarate provides an intriguing possibility for creation of the long-lived 4-spin state as demonstrated by Stevanato et al.[23] In addition, hyperpolarized fumarate is often used in preclinical MRI studies as an in vivo probe for cell necrosis and can be produced by inexpensive parahydrogen-induced polarization technique. Further studies of [2,3-$^{13}C_2$]-fumarate are certainly warranted in combination with ZULF NMR techniques and hyperpolarization.

We also investigated the possibility of detecting [1-$^{13}$C]-glucose using zero-field NMR. Despite the fact that glucose contains many spins and the spectrum is expected to be complicated, the largest heteronuclear coupling is between a single proton and the labeled carbon atom, thus, a cluster of peaks is expected centered around the one-bond $J$-coupling frequency. However, in practice, we observe two featureless humps corresponding to the proton-carbon $J$-coupling frequencies for the $\alpha$- and $\beta$-forms of glucose; no further substructure is resolved [Fig. 2(c)]. The assignment is confirmed by the literature values of $J$-couplings for diastereomers of glucose (Table S1) as well as the fact that corresponding integrals from the $J$-spectrum match expected proportions of $\alpha$- and $\beta$-forms in neural solution at 25 $^o$C as $\sim$1:2, respectively. The ability to observe glucose and distinguish its isomeric forms in solution by ZULF NMR using an inexpensive and portable setup is promising, especially given recent demonstration of hyperpolarization of sugars using SABRE-Relay technique.[24]

The collected spectra match the simulation for the spin systems obtained by numerical diagonalization of the density matrix performed in the SpinDynamica package (Wolfram Mathematica).[22] In general, for small biomolecules containing $^{13}$C, $^{15}$N, and $^{1}$H nuclei, the whole $J$-spectrum is expected to be visible within the detection bandwidth of optical magnetometer since typical $J$-coupling values are less than 300 Hz. The specific spectral line positions are dependent on both the $J$-coupling values and spin-system topologies. A number of approaches can be used to understand and predict spectra under ZULF conditions: (i) analytical diagonalization of the Hamiltonian for simple $AX_n$ spin systems, (ii) perturbation theory (which works well for more complicated spectra with clear hierarchy of coupling strengths and/or residual Zeeman interactions)[3,19] or (iii) numerical diagonalization of the Hamiltonian, doable readily for spin systems up to 12-13 spins 1/2 on regular PCs).[22,25] Agreement between simulated and measured spectra combined with narrow linewidths under ZULF conditions enables chemical identification of biomolecules in liquids, and combination with hyperpolarization techniques is poised to be especially promising.[26]

The coupling constants extracted for [1-$^{13}$C]-glycine, [2,3-$^{13}C_2$]-fumarate, and [1-$^{13}$C]-

D-glucose, extracted by matching the experimentally observed and simulated spectra, correlate well with those obtained from the literature. However, we should note that while it is possible to obtain high-resolution zero-field spectra of these important biomolecules in solution, the obtained signal-to-noise ratio (SNR) is low, necessitating hundreds of averages. In addition, we have worked with highly concentrated (1-10 M) solutions and 50-100% isotopically-enriched samples. For practical analytical applications of portable ZULF apparatus, hyperpolarization is necessary to distinguish molecules at low concentration.

## Near-zero-field relaxometry

ZULF NMR offers a complementary approach to $J$-spectroscopy for studying biomolecules by measuring spin-relaxation times. An important feature of this approach is that relaxation measurements do not necessarily rely on the presence of heteronuclear couplings in the molecule; the measurements can be performed in the presence of a small bias field leading to the appearance of low-frequency resonances [for example, as in Fig. 2(a)].[16,27] In such a case, the relaxation information is extracted from investigation of the properties of the low-frequency signals. Moreover, the effect of the studied molecule on the relaxation properties of the solvent (i.e., measuring magnetization precession of the solvent nuclear spins) can enable indirect studies of low-concentration samples. Since protons possess a high gyromagnetic ratio, such measurements are ideally realized in protonated solvents, avoiding the need of costly deuterated solvents typically employed in high-field NMR.

Ultralow-field relaxometry was implemented with our portable ZULF NMR spectrometer in a manner similar to the studies previously published.[28] Before a measurement, a prepolarized sample is held in a controllable magnetic field for a variable storage time. After this period, this guiding field is switched off and the magnetization signal is recorded. The sequence is repeated with incremented storage time, and the signal amplitude is plotted versus the storage time to extract $T_1$ values from the fit. While the storage is performed in longitudinal magnetic field, a small transverse magnetic field can be turned on during the measurement to enable differentiation of relaxation properties of different resonances in $J$-spectra.

A measurement of [$^{13}$C]-formic acid, performed in such a way is shown in Fig. 3. The storage field was set to 1 $\mu$T while a transverse field of 35 nT was used during the measurement. Under these conditions, the Zeeman interaction is a small perturbation to the strong $J$-coupling, and the ZULF NMR spectrum consists of one low-frequency peak at the average of the $^1$H and $^{13}$C Larmor frequencies and two high-frequency peaks around $J$-coupling value separated by a sum of the Larmor frequencies of the two coupled nuclei (Fig. 3).

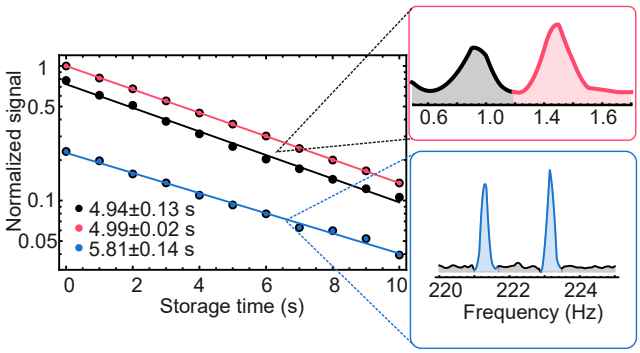


Figure 3: Relaxometry of neat [$^{13}$C]-formic acid. The storage magnetic field was 1 $\mu$T, the measurements were carried out in the presence of a transverse magnetic field (35 nT). Black circles correspond to signal at an average $^1$H-$^{13}$C Larmor frequency, red circles correspond to signal amplitudes at the proton Larmor frequency, blue circles correspond to a signal components around the $^1$H-$^{13}$C $J$-coupling value (222.2 Hz). Insets show parts of the experimental spectrum corresponding to low- and high-frequency peaks. The longitudinal $T_1$ times extracted from both low-frequency components are the same within experimental uncertainty, while the value extracted from high-frequency signal are nearly 20% longer.

In addition to the formic-acid resonances, the low-frequency part of the spectrum exhibits a peak at the proton Larmor frequency, originating from uncoupled acidic protons. Fig-

ure 3 shows relaxation parameters measured for all spectral components as indicated in the insets. Each data-point corresponds to a single collected spectrum, the amplitude was estimated by numerically integrating area under each peak. The extracted values of $T_1$ for both low-frequency spectral features were found to be the same within experimental uncertainty and equal to about 5 s while for the split peak at $J$-coupling value, the longitudinal relaxation time is longer, 5.81±0.14 s. The longer relaxation time of the multiplets near the $J$-coupling frequency is in agreement with previously published data that demonstrated $T_1$ of 5.8±0.1 s for the formic acid sample containing residual amount of water.[29]

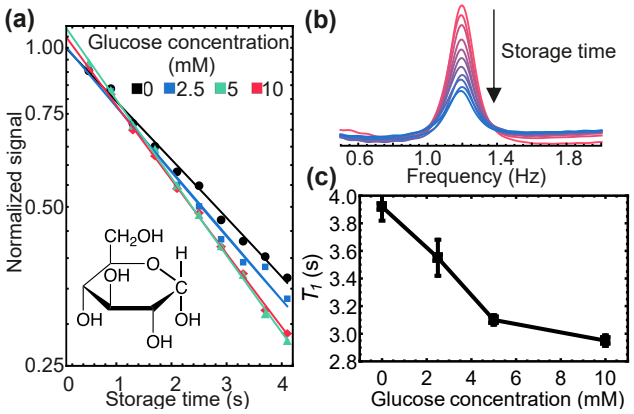


Figure 4: (a) Ultralow-field relaxometry measurements for glucose solutions in water at 1 $\mu$T field. Exponential decay of the signal amplitude is plotted on logarithmic scale. (b) Proton-precession signal detected at a transverse field of 50 nT was obtained while increasing storage time (at 1 $\mu$T). (c) $T_1$ times extracted from the data presented in part (a) for different concentrations of glucose.

On the contrary, the equality of relaxation times for the two peaks at low frequency is surprising since these peaks correspond to magnetization of two different nuclear spin groups ($^1$H-$^{13}$C vs. $^1$H). Investigation of the exact reason to why this is the case goes beyond the scope of this paper but indicates the equality of relaxation mechanisms for the magnetization of two different chemical groups at near-zero-field conditions. In general, the presented protocol enables straightforward measurements of relaxation dispersion from zero field up to the saturation field of mu-metal shields.

To investigate the feasibility of quantifying glucose in aqueous solutions without relying on $J$-spectra, we performed relaxometry measurements of $H_2O$ proton Larmor precession signal as a function of glucose concentration. Example of such a measurement is presented in Fig. 4, where relaxation of protons in water is plotted as a function of glucose concentration in the range of 1-10 mM. Figure 4(a) shows decay of the signal when increasing storage time (up to 4 s), while the Fig. 4(b,c) shows that $T_1$ of water is clearly affected by concentration of dissolved D-glucose.

While these results clearly demonstrate that glucose alone can affect relaxation of water in physiological concentration range, further studies of biological fluids such as plasma, serum, and whole blood are warranted to investigate the feasibility of identifying correlations between metabolic disorders and proton relaxation times of biological fluids. Indeed, it was shown that metabolic syndrome (abnormalities that increases the risk for type 2 diabetes and atherosclerosis) strongly correlate with shortened values of $T_2$ in plasma and serum.[30] In whole blood, $T_2$ was shown to be sensitive to hemoglobin content and oxygenation.[31] Therefore, it is expected that near-zero-field relaxometry will also provide opportunity to probe correlations between relaxation time and metabolic disorders and abnormalities.

Compact ZULF NMR relaxometry based on inexpensive OPM-based sensors such as presented in this work, could further lower the barrier toward compact (and potentially non-invasive) blood tests for candidiasis, hemostasis, malaria and insulin resistance and for population screening and metabolic health assessment for diabetes and prediabetes prevention.[32] In addition, ex vivo identification of biological markers associated with water $T_2$ abnormalities can be probed by these easy-to-handle portable spectroscopic tools.[33]

# Experimental setup

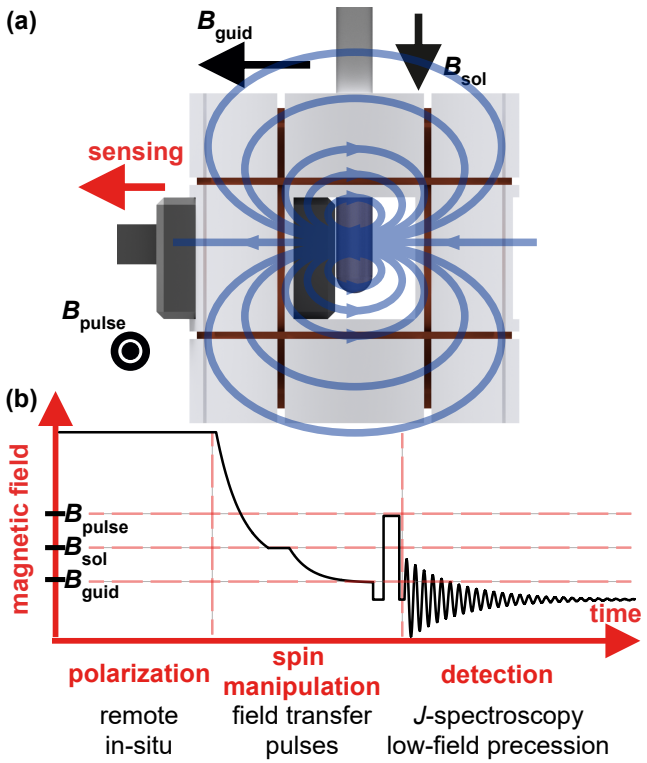


Figure 5: (a) Scheme of the ZULF NMR system. The heart of the ZULF NMR spectrometer, OPM (black), is placed next to the NMR tube (blue), which is surrounded by a frame (white) supporting magnetic-field coils. The polarized sample produces dipolar magnetic field (indicated by blue arrows), which can be detected with the OPM (its sensitive axis is indicated by red arrow). Several magnetic fields (black arrows) are applied to the sample during the measurements: solenoid field ($B_{\mathrm{sol}}$), guiding field in the coil ($B_{\mathrm{guid}}$), and pulsing field ($B_{\mathrm{pulse}}$). (b) The experimental sequence used to detect zero-field spectra: (i) polarization, when the sample is exposed to static magnetic field, (ii) spin manipulations, when the sample is transported from strong to zero field and may subsequently be subjected to magnetic field pulses, and (iii) detection, when the field from the sample is detected with the OPM.

Our ZULF NMR setup is presented in Fig. 5. It is based on a commercial spin-exchange relaxation-free magnetometer magnetometer QuSpin-QZFM.[8] The vapor cell is placed approximately 9.5 mm from the sample enclosed in a regular 5 mm NMR tube. The high sensitivity of the magnetometer (about 15 fT/Hz$^{1/2}$) and a small distance between the cell and the sample are crucial for detection of weak NMR signals under ZULF conditions. It is worth mentioning that despite operating at an elevated temperature (the vapor cell is heated up to 150°C), the QuSpin sensor remains relatively cool (40°C) on the outside, not introducing the problems of heating up the sample, which would be particularly problematic when investigating chemical reactions in which temperature dependence can be significant. The sensor and the sample are enclosed in a multilayer mu-metal magnetic shielding (Twinleaf MS1), separating a region of ZULF conditions from the environmental magnetic fields (the Earth magnetic field, AC-line induced fields, etc.). Typical external field attenuation lays in the range between $10^5$ and $10^6$, while the residual fields can be further reduced with a set of magnetic-field coils mounted inside the shield. In principle, the shield can be replaced with a cheaper construction consisting of single-layer shielding and/or active field compensation exploiting a set of magnetic-field coils,[34,35] offering, however, somewhat worse performance.

For thermal measurements in zero-field NMR, one needs to polarize the sample in a strong external field. In our experiment, a sample is mechanically transported from the Halbach magnet assembly (1.4 T) to the shield within about 200 ms. To provide a guiding field for the transport between two magnetic-field regions and hence ensure well-defined polarization direction inside the shield, a solenoid is wrapped around the whole length of the shuttling path. The magnetic field produced by a solenoid ($B_{\mathrm{sol}}$) is adiabatically switched off to allow spins in the sample to follow the guiding field ($B_{\mathrm{guid}}$) produced by smaller Helmholtz coils wound around the sensor assembly inside the shield [Fig. 5(a)], thus, orienting themselves along the sensing direction of the magnetic-field sensor. In a typical ZULF NMR spectroscopic measurement, the sensitive direction of the sensor (here $z$ direction) coincides with the direction of the guiding field right before transitioning to zero-field conditions [Fig. 5(b)]. This enables efficient de-

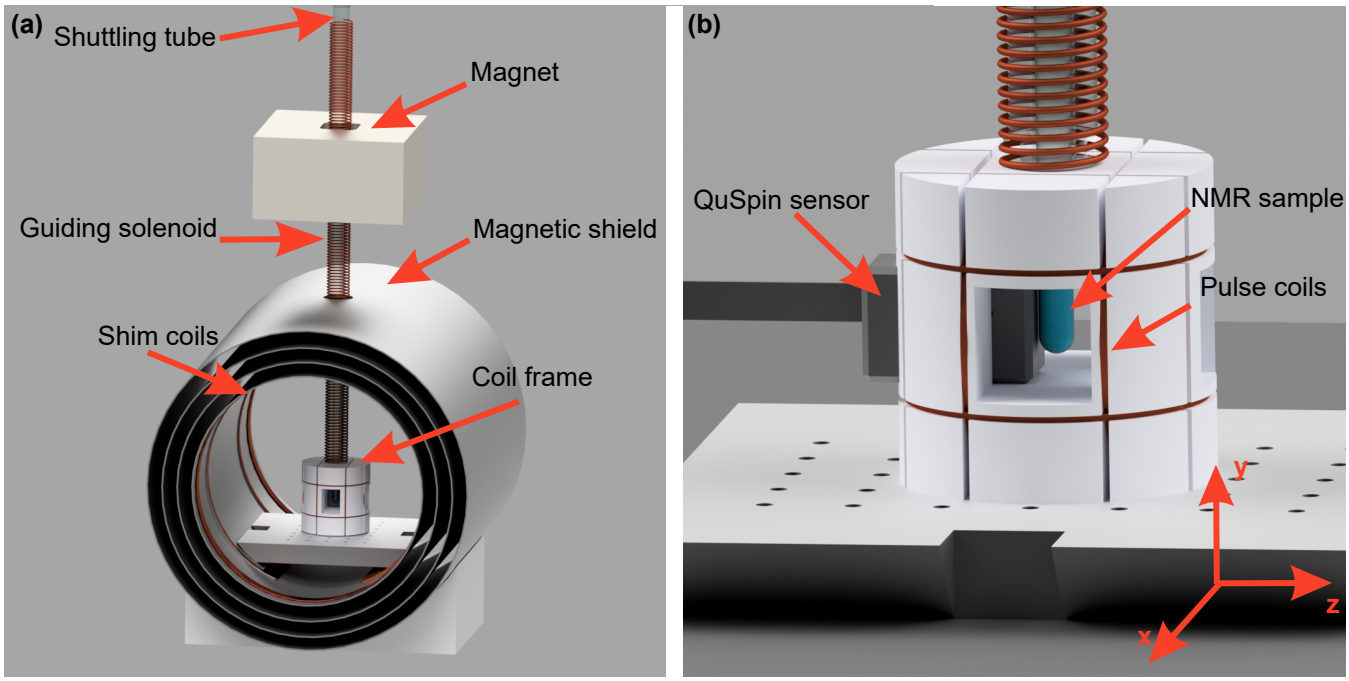


Figure 6: Key components of the experimental setup used in the study. (a) General view of the setup (with magnetic-shield endcaps removed), showing the prepolarizing magnet, solenoid wrapped around the shuttling tube, magnetic shielding, coil frame holding the sensor, and the sample during the measurement. (b) Detailed view of the central part of the system including the coil assembly, magnetometer, and NMR sample (position during the detection stage).

tection of an oscillating magnetic field produced by the sample along the direction of the guiding field.

The field switching is performed using a standard relay board (Himalayan Solutions 8 Channel Relay Module) and to achieve an adiabatic field quench, appropriate capacitor and resistor were added to the coil circuit. After the transfer to zero field, a magnetic-field pulse (typically, a DC field) can be applied in one of three spatial directions. The pulsing is done via high voltage relays (Willamette MHVSW-002V) with a home-built control board. The built pulsing system consists of 6 relays enabling pulsing with arbitrary polarization (DC pulse phase change is done by reversing polarity of the applied field). The set of coils mounted inside the inner most layer is powered by low-noise current source (Twinleaf CSB-03) and is used to precisely control the magnetic field at the position of the NMR sample (see shimming procedure presented in Supplementary Materials). Data acquisition and experimental control is performed using using a data acquisition (DAQ) card (National Instruments 6229). The DAQ card provides triggers for data acquisition (typically 1000 samples/s), issues 5-V logic for controlling relays, and provides timed counter gating magnetic field pulses. After prepolarization and completing the measurements, the NMR sample is shuttled back into the Halbach magnet.

The setup described in this work [Fig. 6] was placed on a small and easy-to-move cart [Fig. SI 3]. Since the QuSpin sensor is a solid package, moving the system does not cause any misalignment or degradation in performance. The setup is modular, i.e., every part can be easily removed or replaced. For example, the prepolarizaing magnet can be removed and the system for parahydrogen-induced polarization (PHIP) can be implemented. This modularity also allows one to easily disassemble the system for diagnostic purposes. The presented device was put together from readily available parts (a commercial sensor, magnetic shielding, a Halbach magnet, a pump, a DAQ system and a current source); development of more compact

systems is in progress.

# Conclusions

In conclusion, in this work we constructed a portable zero-field NMR spectrometer based on commercially available magnetometer and measured the spectra of small biomolecules: [$^{13}$C]-formic acid, [1-$^{13}$C]-glycine, [2,3-$^{13}$C]-fumarate, and [1$^{13}$C]-glucose both at zero-field ($J$-spectra) and at near-zero-field conditions (employed for spin relaxometry). We present a measurement approach where the transverse magnetic field is used during the detection and describe rationale behind it for the analysis of biomolecules in solution. We investigated the feasibility of indirect glucose-concentration measurements in water by analysing water relaxation time as a function of the concentration. These results are promising for the detection of small biomolecules in physiological liquids and are synergistically compatible with inexpensive hyperpolarization techniques utilizing parahydrogen (e.g., PHIP, SABRE, SABRE-Relay) paving a way for portable inexpensive ZULF NMR sensors with applications beyond chemical laboratory.

**Acknowledgement** We gratefully acknowledge the financial support by NSF CHE-1709944, funding from the European Union's Horizon 2020 research, and Alexander von Humboldt Foundation in the framework of the Sofja Kovalevskaja Award. SP and PP acknowledge the support from the grants of the National Science Centre, Poland within the OPUS program (Project No. 2015/19/B/ST2/02129). DB acknowledges support by the Cluster of Excellence Precision Physics, Fundamental Interactions, and Structure of Matter (PRISMA+ EXC 2118/1) funded by the DFG within the German Excellence Strategy (Project ID 39083149).

# References

(1) Ledbetter, M.; Savukov, I.; Budker, D.; Shah, V.; Knappe, S.; Kitching, J.; Michalak, D.; Xu, S.; Pines, A. Zero-field remote detection of NMR with a microfabricated atomic magnetometer. *Proceedings of the National Academy of Sciences* **2008**, *105*, 2286–2290.

(2) Ledbetter, M.; Crawford, C.; Pines, A.; Wemmer, D.; Knappe, S.; Kitching, J.; Budker, D. Optical detection of NMR J-spectra at zero magnetic field. *Journal of magnetic resonance* **2009**, *199*, 25–29.

(3) Ledbetter, M.; Theis, T.; Blanchard, J.; Ring, H.; Ganssle, P.; Appelt, S.; Blümich, B.; Pines, A.; Budker, D. Near-zero-field nuclear magnetic resonance. *Physical Review Letters* **2011**, *107*, 107601.

(4) Theis, T.; Ganssle, P.; Kervern, G.; Knappe, S.; Kitching, J.; Ledbetter, M.; Budker, D.; Pines, A. Parahydrogen-enhanced zero-field nuclear magnetic resonance. *Nature Physics* **2011**, *7*, 571–575.

(5) Theis, T.; Ledbetter, M. P.; Kervern, G.; Blanchard, J. W.; Ganssle, P. J.; Butler, M. C.; Shin, H. D.; Budker, D.; Pines, A. Zero-field NMR enhanced by parahydrogen in reversible exchange. *Journal of the American Chemical Society* **2012**, *134*, 3987–3990.

(6) Blanchard, J. W.; Budker, D. Zero-to Ultralow-Field NMR. *eMagRes* **2016**, 1395–1410.

(7) Tayler, M. C.; Theis, T.; Sjolander, T. F.; Blanchard, J. W.; Kentner, A.; Pustelny, S.; Pines, A.; Budker, D. Invited Review Article: Instrumentation for nuclear magnetic resonance in zero and ultralow magnetic field. *Review of Scientific Instruments* **2017**, *88*, 091101.

(8) Blanchard, J. W.; Wu, T.; Eills, J.; Hu, Y.; Budker, D. Zero-to ultralow-field nuclear magnetic resonance J-spectroscopy with commercial atomic magnetometers. *Journal of Magnetic Resonance* **2020**, 106723.

(9) Theis, T.; Blanchard, J. W.; Butler, M. C.; Ledbetter, M. P.; Budker, D.; Pines, A. Chemical analysis using J-coupling multiplets in zero-field NMR. *Chemical Physics Letters* **2013**, *580*, 160–165.

(10) Blanchard, J. W.; Ledbetter, M. P.; Theis, T.; Butler, M. C.; Budker, D.; Pines, A. High-resolution zero-field NMR J-spectroscopy of aromatic compounds. *Journal of the American Chemical Society* **2013**, *135*, 3607–3612.

(11) Blanchard, J. W.; Sjolander, T. F.; King, J. P.; Ledbetter, M. P.; Levine, E. H.; Bajaj, V. S.; Budker, D.; Pines, A. Measurement of untruncated nuclear spin interactions via zero-to ultralow-field nuclear magnetic resonance. *Physical Review B* **2015**, *92*, 220202.

(12) Barskiy, D. A.; Tayler, M. C.; Marco-Rius, I.; Kurhanewicz, J.; Vigneron, D. B.; Cikrikci, S.; Aydogdu, A.; Reh, M.; Pravdivtsev, A. N.; Hövener, J.-B., et al. Zero-field nuclear magnetic resonance of chemically exchanging systems. *Nature communications* **2019**, *10*, 1–9.

(13) Burueva, D. B.; Eills, J.; Blanchard, J. W.; Garcon, A.; Picazo-Frutos, R.; Kovtunov, K. V.; Koptyug, I. V.; Budker, D. Chemical reaction monitoring using zero-field nuclear magnetic resonance enables study of heterogeneous samples in metal containers. *Angewandte Chemie International Edition* **2020**,

(14) Sjolander, T. F.; Blanchard, J. W.; Budker, D.; Pines, A. Two-Dimensional Single-and Multiple-Quantum Correlation Spectroscopy in Zero-Field Nuclear Magnetic Resonance. *Journal of Magnetic Resonance* **2020**, *318*, 106781.

(15) Ledbetter, M.; Theis, T.; Blanchard, J.; Ring, H.; Ganssle, P.; Appelt, S.; Blumich, B.; Pines, A.; Budker, D. Near-zero-field nuclear magnetic resonance. *Physical Review Letters* **2011**, *107*, 107601.

(16) Tayler, M. C.; Ward-Williams, J.; Gladden, L. F. NMR relaxation in porous materials at zero and ultralow magnetic fields. *Journal of Magnetic Resonance* **2018**, *297*, 1–8.

(17) Allred, J.; Lyman, R.; Kornack, T.; Romalis, M. V. High-sensitivity atomic magnetometer unaffected by spin-exchange relaxation. *Physical Review Letters* **2002**, *89*, 130801.

(18) Kimball, D. F. J.; Budker, D. *Optical Magnetometry*; Cambridge University Press, 2013.

(19) Butler, M. C.; Ledbetter, M. P.; Theis, T.; Blanchard, J. W.; Budker, D.; Pines, A. Multiplets at zero magnetic field: The geometry of zero-field NMR. *The Journal of Chemical Physics* **2013**, *138*, 184202.

(20) Theis, T.; Blanchard, J. W.; Butler, M. C.; Ledbetter, M. P.; Budker, D.; Pines, A. Chemical analysis using J-coupling multiplets in zero-field NMR. *Chemical Physics Letters* **2013**, *580*, 160–165.

(21) Tayler, M. C.; Gladden, L. F. Scalar relaxation of NMR transitions at ultralow magnetic field. *Journal of Magnetic Resonance* **2019**, *298*, 101 – 106.

(22) Bengs, C.; Levitt, M. H. SpinDynamica: Symbolic and numerical magnetic resonance in a Mathematica environment. *Magnetic Resonance in Chemistry* **2018**, *56*, 374–414.

(23) Stevanato, G.; Roy, S. S.; Hill-Cousins, J.; Kuprov, I.; Brown, L. J.; Brown, R. C.; Pileio, G.; Levitt, M. H. Long-lived nuclear spin states far from magnetic equivalence. *Physical Chemistry Chemical Physics* **2015**, *17*, 5913–5922.

(24) Richardson, P. M.; Iali, W.; Roy, S. S.; Rayner, P. J.; Halse, M. E.; Duckett, S. B. Rapid 13 C NMR hyperpolarization delivered from para-hydrogen enables the

low concentration detection and quantification of sugars. *Chemical Science* **2019**, *10*, 10607–10619.

(25) Wilzewski, A.; Afach, S.; Blanchard, J. W.; Budker, D. A method for measurement of spin-spin couplings with sub-mHz precision using zero-to ultralow-field nuclear magnetic resonance. *Journal of Magnetic Resonance* **2017**, *284*, 66–72.

(26) Knecht, S.; Blanchard, J. W.; Barskiy, D.; Cavallari, E.; Dagys, L.; van Dyke, E.; Tsukanov, M.; Bliemel, B.; Münnemann, K.; Aime, S., et al. Rapid Hyperpolarization and Purification of the Metabolite Fumarate in Aqueous Solution. **2020**,

(27) Tayler, M. C.; Ward-Williams, J.; Gladden, L. F. Ultralow-field nuclear magnetic resonance of liquids confined in ferromagnetic and paramagnetic materials. *Applied Physics Letters* **2019**, *115*, 072409.

(28) Ganssle, P. J.; Shin, H. D.; Seltzer, S. J.; Bajaj, V. S.; Ledbetter, M. P.; Budker, D.; Knappe, S.; Kitching, J.; Pines, A. Ultra-Low-Field NMR Relaxation and Diffusion Measurements Using an Optical Magnetometer. *Angewandte Chemie International Edition* **2014**, *53*, 9766–9770.

(29) Emondts, M.; Ledbetter, M. P.; Pustelny, S.; Theis, T.; Patton, B.; Blanchard, J. W.; Butler, M. C.; Budker, D.; Pines, A. Long-lived heteronuclear spin-singlet states in liquids at a zero magnetic field. *Physical Review Letters* **2014**, *112*, 077601.

(30) Robinson, M. D.; Mishra, I.; Deodhar, S.; Patel, V.; Gordon, K. V.; Vintimilla, R.; Brown, K.; Johnson, L.; O'Bryant, S.; Cistola, D. P. Water $T_2$ as an early, global and practical biomarker for metabolic syndrome: an observational cross-sectional study. *Journal of translational medicine* **2017**, *15*, 258.

(31) Cistola, D. P.; Robinson, M. D. Compact NMR relaxometry of human blood and blood components. *TrAC Trends in Analytical Chemistry* **2016**, *83*, 53–64.

(32) Mishra, I.; Jones, C.; Patel, V.; Deodhar, S.; Cistola, D. P. Early detection of metabolic dysregulation using water T2 analysis of biobanked samples. *Diabetes, Metabolic Syndrome and Obesity: Targets and Therapy* **2018**, *11*, 807.

(33) Patel, V.; Dwivedi, A. K.; Deodhar, S.; Mishra, I.; Cistola, D. P. Aptamer-based search for correlates of plasma and serum water T 2: implications for early metabolic dysregulation and metabolic syndrome. *Biomarker Research* **2018**, *6*, 28.

(34) Savukov, I.; Seltzer, S.; Romalis, M. Detection of NMR signals with a radio-frequency atomic magnetometer. *Journal of Magnetic Resonance* **2007**, *185*, 214–220.

(35) Bevilacqua, G.; Biancalana, V.; Baranga, A. B.-A.; Dancheva, Y.; Rossi, C. Microtesla NMR J-coupling spectroscopy with an unshielded atomic magnetometer. *Journal of Magnetic Resonance* **2016**, *263*, 65–70.

# Graphical TOC Entry